# 16. STRUCTURE FUNCTIONS

Written Summer 2001 by B. Foster (University of Oxford), A.D. Martin (University of Durham), M.G. Vincter (Carleton University). Updated Summer 2005.

## 16.1. Deep inelastic scattering

High energy lepton-nucleon scattering (deep inelastic scattering) plays a key role in determining the partonic structure of the proton. The process $\ell N \to \ell' X$ is illustrated in Fig. 16.1. The filled circle in this figure represents the internal structure of the proton which can be expressed in terms of structure functions.

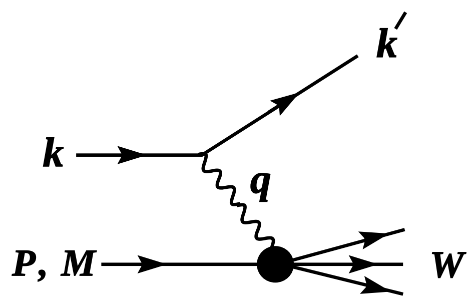


**Figure 16.1:** Kinematic quantities for the description of deep inelastic scattering. The quantities $k$ and $k'$ are the four-momenta of the incoming and outgoing leptons, $P$ is the four-momentum of a nucleon with mass $M$, and $W$ is the mass of the recoiling system $X$. The exchanged particle is a $\gamma$, $W^{\pm}$, or $Z$; it transfers four-momentum $q = k - k'$ to the nucleon.

Invariant quantities:

$\nu = \dfrac{q \cdot P}{M} = E - E'$ is the lepton's energy loss in the nucleon rest frame (in earlier literature sometimes $\nu = q \cdot P$). Here, $E$ and $E'$ are the initial and final lepton energies in the nucleon rest frame.

$Q^2 = -q^2 = 2(EE' - \overrightarrow{k} \cdot \overrightarrow{k}') - m_\ell^2 - m_{\ell'}^2$ where $m_\ell(m_{\ell'})$ is the initial (final) lepton mass. If $EE' \sin^2(\theta/2) \gg m_\ell^2,\, m_{\ell'}^2$, then

$\approx 4EE' \sin^2(\theta/2)$, where $\theta$ is the lepton's scattering angle with respect to the lepton beam direction.

$x = \dfrac{Q^2}{2M\nu}$ where, in the parton model, $x$ is the fraction of the nucleon's momentum carried by the struck quark.

$y = \dfrac{q \cdot P}{k \cdot P} = \dfrac{\nu}{E}$ is the fraction of the lepton's energy lost in the nucleon rest frame.

$W^2 = (P + q)^2 = M^2 + 2M\nu - Q^2$ is the mass squared of the system $X$ recoiling against the scattered lepton.

$s = (k + P)^2 = \dfrac{Q^2}{xy} + M^2 + m_\ell^2$ is the center-of-mass energy squared of the lepton-nucleon system.

The process in Fig. 16.1 is called deep ($Q^2 >> M^2$) inelastic ($W^2 >> M^2$) scattering (DIS). In what follows, the masses of the initial and scattered leptons, $m_\ell$ and $m'_\ell$, are neglected.

**16.1.1. *DIS cross sections*** :

$$\frac{d^2\sigma}{dx\, dy} = x\,(s - M^2)\,\frac{d^2\sigma}{dx\, dQ^2} = \frac{2\pi\, M\nu}{E'}\,\frac{d^2\sigma}{d\Omega_{\rm Nrest}\, dE'} \; . \tag{16.1}$$

In lowest-order perturbation theory, the cross section for the scattering of polarized leptons on polarized nucleons can be expressed in terms of the products of leptonic and hadronic tensors associated with the coupling of the exchanged bosons at the upper and lower vertices in Fig. 16.1 (see Refs. 1–4)

$$\frac{d^2\sigma}{dxdy} \;=\; \frac{2\pi y\alpha^2}{Q^4}\sum_j \eta_j\, L_j^{\mu\nu}\, W_{\mu\nu}^j \; . \tag{16.2}$$

For neutral-current processes, the summation is over $j = \gamma, Z$ and $\gamma Z$ representing photon and $Z$ exchange and the interference between them, whereas for charged-current interactions there is only $W$ exchange, $j = W$. (For transverse nucleon polarization, there is a dependence on the azimuthal angle of the scattered lepton.) $L_{\mu\nu}$ is the lepton tensor associated with the coupling of the exchange boson to the leptons. For incoming leptons of charge $e = \pm 1$ and helicity $\lambda = \pm 1$,

$$\begin{aligned} L^\gamma_{\mu\nu} &= 2\left(k_\mu k'_\nu + k'_\mu k_\nu - k\cdot k' g_{\mu\nu} - i\lambda\varepsilon_{\mu\nu\alpha\beta}k^\alpha k'^\beta\right), \\ L^{\gamma Z}_{\mu\nu} &= (g^e_V + e\lambda g^e_A)\; L^\gamma_{\mu\nu}, \qquad L^Z_{\mu\nu} = (g^e_V + e\lambda g^e_A)^2\; L^\gamma_{\mu\nu}, \\ L^W_{\mu\nu} &= (1 + e\lambda)^2\; L^\gamma_{\mu\nu}, \end{aligned} \tag{16.3}$$

where $g^e_V = -\frac{1}{2} + 2\sin^2\theta_W, \qquad g^e_A = -\frac{1}{2}$ .

Although here the helicity formalism is adopted, an alternative approach is to express the tensors in Eq. (16.3) in terms of the polarization of the lepton.

The factors $\eta_j$ in Eq. (16.2) denote the ratios of the corresponding propagators and couplings to the photon propagator and coupling squared

$$\begin{aligned} \eta_\gamma &= 1 \quad ; \quad \eta_{\gamma Z} = \left(\frac{G_F M_Z^2}{2\sqrt{2}\pi\alpha}\right)\left(\frac{Q^2}{Q^2 + M_Z^2}\right); \\ \eta_Z &= \eta^2_{\gamma Z} \quad ; \quad \eta_W = \frac{1}{2}\left(\frac{G_F M_W^2}{4\pi\alpha}\,\frac{Q^2}{Q^2 + M_W^2}\right)^2 . \end{aligned} \tag{16.4}$$

The hadronic tensor, which describes the interaction of the appropriate electroweak currents with the target nucleon, is given by

$$W_{\mu\nu} \;=\; \frac{1}{4\pi}\int d^4z\; e^{iq\cdot z}\;\left\langle P, S\left|\left[J^\dagger_\mu(z), J_\nu(0)\right]\right|\, P, S\right\rangle, \tag{16.5}$$

where $S$ denotes the nucleon-spin 4-vector, with $S^2 = -M^2$ and $S\cdot P = 0$.

## 16.2. Structure functions of the proton

The structure functions are defined in terms of the hadronic tensor (see Refs. 1–3)

$$\begin{aligned}W_{\mu\nu} = &\left(-g_{\mu\nu} + \frac{q_\mu q_\nu}{q^2}\right) F_1(x,Q^2) + \frac{\hat{P}_\mu \hat{P}_\nu}{P\cdot q} F_2(x,Q^2)\\ &- i\varepsilon_{\mu\nu\alpha\beta}\frac{q^\alpha P^\beta}{2P\cdot q} F_3(x,Q^2)\\ &+ i\varepsilon_{\mu\nu\alpha\beta}\frac{q^\alpha}{P\cdot q}\left[S^\beta g_1(x,Q^2) + \left(S^\beta - \frac{S\cdot q}{P\cdot q} P^\beta\right) g_2(x,Q^2)\right]\\ &+ \frac{1}{P\cdot q}\left[\tfrac{1}{2}\left(\hat{P}_\mu \hat{S}_\nu + \hat{S}_\mu \hat{P}_\nu\right) - \frac{S\cdot q}{P\cdot q}\hat{P}_\mu \hat{P}_\nu\right] g_3(x,Q^2)\\ &+ \frac{S\cdot q}{P\cdot q}\left[\frac{\hat{P}_\mu \hat{P}_\nu}{P\cdot q} g_4(x,Q^2) + \left(-g_{\mu\nu} + \frac{q_\mu q_\nu}{q^2}\right) g_5(x,Q^2)\right]\end{aligned} \tag{16.6}$$

where

$$\hat{P}_\mu = P_\mu - \frac{P\cdot q}{q^2} q_\mu, \qquad \hat{S}_\mu = S_\mu - \frac{S\cdot q}{q^2} q_\mu . \tag{16.7}$$

In Ref. [2], the definition of $W_{\mu\nu}$ with $\mu \leftrightarrow \nu$ is adopted, which changes the sign of the $\varepsilon_{\mu\nu\alpha\beta}$ terms in Eq. (16.6), although the formulae given here below are unchanged. Ref. [1] tabulates the relation between the structure functions defined in Eq. (16.6) and other choices available in the literature.

The cross sections for neutral- and charged-current deep inelastic scattering on unpolarized nucleons can be written in terms of the structure functions in the generic form

$$\begin{aligned}\frac{d^2\sigma^i}{dx\,dy} = \frac{4\pi\alpha^2}{xyQ^2}\eta^i \Bigg\{&\left(1 - y - \frac{x^2y^2M^2}{Q^2}\right) F_2^i\\ &+ y^2 x F_1^i \mp \left(y - \frac{y^2}{2}\right) x F_3^i\Bigg\},\end{aligned} \tag{16.8}$$

where $i$ = NC, CC corresponds to neutral-current ($eN \to eX$) or charged-current ($eN \to \nu X$ or $\nu N \to eX$) processes, respectively. For incoming neutrinos, $L^W_{\mu\nu}$ of Eq. (16.3) is still true, but with $e, \lambda$ corresponding to the outgoing charged lepton. In the last term of Eq. (16.8), the $-$ sign is taken for an incoming $e^+$ or $\overline{\nu}$ and the $+$ sign for an incoming $e^-$ or $\nu$. The factor $\eta^{\rm NC} = 1$ for unpolarized $e^\pm$ beams, whereas*

$$\eta^{\rm CC} = (1 \pm \lambda)^2 \eta_W \tag{16.9}$$

with $\pm$ for $\ell^\pm$; and where $\lambda$ is the helicity of the incoming lepton and $\eta_W$ is defined in Eq. (16.4); for incoming neutrinos $\eta^{\rm CC} = 4\eta_W$. The CC structure functions, which derive exclusively from $W$ exchange, are

$$F_1^{\rm CC} = F_1^W,\ F_2^{\rm CC} = F_2^W,\ xF_3^{\rm CC} = xF_3^W . \tag{16.10}$$

The NC structure functions $F_2^\gamma, F_2^{\gamma Z}, F_2^Z$ are, for $e^\pm N \to e^\pm X$, given by Ref. [5],

$$F_2^{\rm NC} \;=\; F_2^\gamma \;-\; (g_V^e \pm \lambda g_A^e)\eta_{\gamma Z} F_2^{\gamma Z} \;+\; ({g_V^e}^2 + {g_A^e}^2 \pm 2\lambda g_V^e g_A^e)\, \eta_Z F_2^Z \tag{16.11}$$

and similarly for $F_1^{\rm NC}$, whereas

$$xF_3^{\rm NC} = -(g_A^e \pm \lambda g_V^e)\eta_{\gamma Z} xF_3^{\gamma Z} + [2 g_V^e g_A^e \pm \lambda({g_V^e}^2 + {g_A^e}^2)]\eta_Z xF_3^Z \ . \tag{16.12}$$

The polarized cross-section difference

$$\Delta\sigma \;=\; \sigma(\lambda_n = -1, \lambda_\ell) \;-\; \sigma(\lambda_n = 1, \lambda_\ell)\ , \tag{16.13}$$

where $\lambda_\ell, \lambda_n$ are the helicities ($\pm 1$) of the incoming lepton and nucleon, respectively, may be expressed in terms of the five structure functions $g_{1,...5}(x, Q^2)$ of Eq. (16.6). Thus,

$$\begin{aligned}\frac{d^2\Delta\sigma^i}{dx\,dy} \;=\; \frac{8\pi\alpha^2}{xyQ^2}\,\eta^i \Bigg\{ &-\lambda_\ell y \left(2 - y - 2x^2y^2\frac{M^2}{Q^2}\right) x g_1^i + \lambda_\ell 4x^3y^2\,\frac{M^2}{Q^2}\, g_2^i \\ &+\; 2x^2y\frac{M^2}{Q^2}\left(1 - y - x^2y^2\frac{M^2}{Q^2}\right)\, g_3^i \\ &-\; \left(1 + 2x^2y\frac{M^2}{Q^2}\right)\left[\left(1 - y - x^2y^2\frac{M^2}{Q^2}\right)\, g_4^i + xy^2 g_5^i\right]\Bigg\}\end{aligned} \tag{16.14}$$

with $i$ = NC or CC as before. The Eq. (16.13) corresponds to the difference of antiparallel minus parallel spins of the incoming particles for $e^-$ or $\nu$ initiated reactions, but parallel minus antiparallel for $e^+$ or $\overline{\nu}$ initiated processes. For longitudinal nucleon polarization, the contributions of $g_2$ and $g_3$ are suppressed by powers of $M^2/Q^2$. These structure functions give an unsuppressed contribution to the cross section for transverse polarization [1], but in this case the cross-section difference vanishes as $M/Q \to 0$.

Because the same tensor structure occurs in the spin-dependent and spin-independent parts of the hadronic tensor of Eq. (16.6) in the $M^2/Q^2 \to 0$ limit, the differential cross-section difference of Eq. (16.14) may be obtained from the differential cross section Eq. (16.8) by replacing

$$F_1 \;\to\; -g_5\ , \quad F_2 \;\to\; -g_4\ , \quad F_3 \;\to\; 2g_1\ , \tag{16.15}$$

and multiplying by two, since the total cross section is the average over the initial-state polarizations. In this limit, Eq. (16.8) and Eq. (16.14) may be written in the form

$$\begin{aligned}\frac{d^2\sigma^i}{dx\,dy} &= \frac{2\pi\alpha^2}{xyQ^2}\,\eta^i\left[Y_+ F_2^i \mp Y_- xF_3^i - y^2 F_L^i\right], \\ \frac{d^2\Delta\sigma^i}{dx\,dy} &= \frac{4\pi\alpha^2}{xyQ^2}\,\eta^i\left[-Y_+ g_4^i \mp Y_- 2xg_1^i + y^2 g_L^i\right],\end{aligned} \tag{16.16}$$

with $i$ = NC or CC, where $Y_\pm = 1 \pm (1-y)^2$ and

$$F_L^i \;=\; F_2^i \;-\; 2xF_1^i\ , \qquad g_L^i \;=\; g_4^i \;-\; 2xg_5^i\ . \tag{16.17}$$

In the naive quark-parton model, the analogy with the Callan-Gross relations [6] $F_L^i = 0$, are the Dicus relations [7] $g_L^i = 0$. Therefore, there are only two independent polarized structure functions: $g_1$ (parity conserving) and $g_5$ (parity violating), in analogy with the unpolarized structure functions $F_1$ and $F_3$.

**16.2.1. *Structure functions in the quark-parton model*:**

In the quark-parton model [8,9], contributions to the structure functions $F^i$ and $g^i$ can be expressed in terms of the quark distribution functions $q(x,Q^2)$ of the proton, where $q = u, \overline{u}, d, \overline{d}$ etc. The quantity $q(x,Q^2)dx$ is the number of quarks (or antiquarks) of designated flavor that carry a momentum fraction between $x$ and $x+dx$ of the proton's momentum in a frame in which the proton momentum is large.

For the neutral-current processes $ep \to eX$,

$$\begin{aligned}
\left[F_2^{\gamma},\, F_2^{\gamma Z},\, F_2^{Z}\right] &= x\sum_q \left[e_q^2,\, 2e_q g_V^q,\, {g_V^q}^2 + {g_A^q}^2\right] (q+\overline{q}) \ ,\\
\left[F_3^{\gamma},\, F_3^{\gamma Z},\, F_3^{Z}\right] &= \sum_q \left[0,\, 2e_q g_A^q,\, 2g_V^q g_A^q\right] (q-\overline{q}) \ ,\\
\left[g_1^{\gamma},\, g_1^{\gamma Z},\, g_1^{Z}\right] &= \frac{1}{2}\sum_q \left[e_q^2,\, 2e_q g_V^q,\, {g_V^q}^2 + {g_A^q}^2\right] (\Delta q+\Delta\overline{q}) \ ,\\
\left[g_5^{\gamma},\, g_5^{\gamma Z},\, g_5^{Z}\right] &= \sum_q \left[0,\, e_q g_A^q,\, g_V^q g_A^q\right] (\Delta q-\Delta\overline{q}) \ ,
\end{aligned} \tag{16.18}$$

where $g_V^q = \pm\frac{1}{2} - 2e_q \sin^2\theta_W$ and $g_A^q = \pm\frac{1}{2}$, with $\pm$ according to whether $q$ is a $u-$ or $d-$type quark respectively. The quantity $\Delta q$ is the difference $q\uparrow - q\downarrow$ of the distributions with the quark spin parallel and antiparallel to the proton spin.

For the charged-current processes $e^-p \to \nu X$ and $\overline{\nu}p \to e^+X$, the structure functions are:

$$\begin{aligned}
F_2^{W^-} &= 2x(u+\overline{d}+\overline{s}+c\ldots) \ ,\\
F_3^{W^-} &= 2(u-\overline{d}-\overline{s}+c\ldots) \ ,\\
g_1^{W^-} &= (\Delta u+\Delta\overline{d}+\Delta\overline{s}+\Delta c\ldots) \ ,\\
g_5^{W^-} &= (-\Delta u+\Delta\overline{d}+\Delta\overline{s}-\Delta c\ldots) \ ,
\end{aligned} \tag{16.19}$$

where only the active flavors are to be kept and where CKM mixing has been neglected. For $e^+p \to \overline{\nu}X$ and $\nu p \to e^-X$, the structure functions $F^{W^+}, g^{W^+}$ are obtained by the flavor interchanges $d \leftrightarrow u, s \leftrightarrow c$ in the expressions for $F^{W^-}, g^{W^-}$. The structure functions for scattering on a neutron are obtained from those of the proton by the interchange $u \leftrightarrow d$. For both the neutral- and charged-current processes, the quark-parton model predicts $2xF_1^i = F_2^i$ and $g_4^i = 2xg_5^i$.

Neglecting masses, the structure functions $g_2$ and $g_3$ contribute only to scattering from transversely polarized nucleons (for which $S \cdot q = 0$), and have no simple interpretation in terms of the quark-parton model. They arise from off-diagonal matrix elements $\langle P,\lambda'|[J_\mu^\dagger(z), J_\nu(0)]|P,\lambda\rangle$, where the proton helicities satisfy $\lambda' \neq \lambda$. In fact, the leading-twist contributions to both $g_2$ and $g_3$ are both twist-2 and twist-3, which contribute at the same order of $Q^2$. The Wandzura-Wilczek relation [10] expresses the twist-2 part of

$g_2$ in terms of $g_1$ as

$$g_2^i(x) \;=\; -g_1^i(x) \;+\; \int_x^1 \frac{dy}{y}\, g_1^i(y)\;. \tag{16.20}$$

However, the twist-3 component of $g_2$ is unknown. Similarly, there is a relation expressing the twist-2 part of $g_3$ in terms of $g_4$. A complete set of relations, including $M^2/Q^2$ effects, can be found in Ref. [11].

### 16.2.2. *Structure functions and QCD* :

One of the most striking predictions of the quark-parton model is that the structure functions $F_i, g_i$ *scale*, *i.e.*, $F_i(x,Q^2) \to F_i(x)$ in the Bjorken limit that $Q^2$ and $\nu \to \infty$ with $x$ fixed [12]. This property is related to the assumption that the transverse momentum of the partons in the infinite-momentum frame of the proton is small. In QCD, however, the radiation of hard gluons from the quarks violates this assumption, leading to logarithmic scaling violations, which are particularly large at small $x$, see Fig. 16.2. The radiation of gluons produces the evolution of the structure functions. As $Q^2$ increases, more and more gluons are radiated, which in turn split into $q\overline{q}$ pairs. This process leads both to the softening of the initial quark momentum distributions and to the growth of the gluon density and the $q\overline{q}$ sea as $x$ decreases.

In QCD, the above process is described in terms of scale-dependent parton distributions $f_a(x,\mu^2)$, where $a = g$ or $q$ and, typically, $\mu$ is the scale of the probe $Q$. For $Q^2 \gg M^2$, the structure functions are of the form

$$F_i = \sum_a C_i^a \otimes f_a, \tag{16.21}$$

where $\otimes$ denotes the convolution integral

$$C \;\otimes\; f \;=\; \int_x^1 \frac{dy}{y}\, C(y)\, f\left(\frac{x}{y}\right)\;, \tag{16.22}$$

and where the coefficient functions $C_i^a$ are given as a power series in $\alpha_s$. The parton distribution $f_a$ corresponds, at a given $x$, to the density of parton $a$ in the proton integrated over transverse momentum $k_t$ up to $\mu$. Its evolution in $\mu$ is described in QCD by a DGLAP equation (see Refs. 14–17) which has the schematic form

$$\frac{\partial f_a}{\partial \ln \mu^2} \sim \frac{\alpha_s(\mu^2)}{2\pi} \sum_b \left(P_{ab} \otimes f_b\right)\;, \tag{16.23}$$

where the $P_{ab}$, which describe the parton splitting $b \to a$, are also given as a power series in $\alpha_s$. Although perturbative QCD can predict, via Eq. (16.23), the evolution of the parton distribution functions from a particular scale, $\mu_0$, these DGLAP equations cannot predict them *a priori* at any particular $\mu_0$. Thus they must be measured at a starting point $\mu_0$ before the predictions of QCD can be compared to the data at other scales, $\mu$. In general, all observables involving a hard hadronic interaction (such as structure

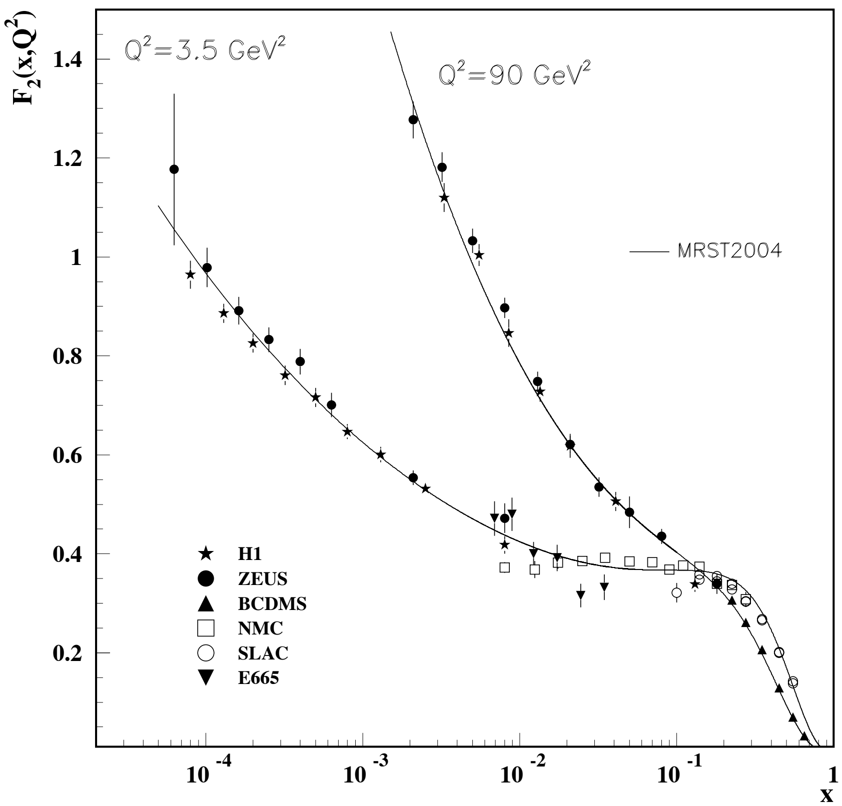


**Figure 16.2:** The proton structure function $F_2^p$ given at two $Q^2$ values (3.5 GeV$^2$ and 90 GeV$^2$), which exhibit scaling at the 'pivot' point $x \sim 0.14$. See the caption in Fig. 16.6 for the references of the data. Also shown is the MRST2004 parameterization [13] given at the same scales.

functions) can be expressed as a convolution of calculable, process-dependent coefficient functions and these universal parton distributions, e.g. Eq. (16.21).

It is often convenient to write the evolution equations in terms of the gluon, non-singlet ($q^{NS}$) and singlet ($q^S$) quark distributions, such that

$$q^{NS} = q_i - \overline{q}_i \quad (\text{or } q_i - q_j), \qquad q^S = \sum_i (q_i + \overline{q}_i) \ . \tag{16.24}$$

The non-singlet distributions have non-zero values of flavor quantum numbers, such as isospin and baryon number. The DGLAP evolution equations then take the form

$$\frac{\partial q^{NS}}{\partial \ln \mu^2} = \frac{\alpha_s(\mu^2)}{2\pi} P_{qq} \otimes q^{NS} \ ,$$

$$\frac{\partial}{\partial \ln \mu^2} \begin{pmatrix} q^S \\ g \end{pmatrix} = \frac{\alpha_s(\mu^2)}{2\pi} \begin{pmatrix} P_{qq} & 2n_f\, P_{qg} \\ P_{gq} & P_{gg} \end{pmatrix} \otimes \begin{pmatrix} q^S \\ g \end{pmatrix} \ , \tag{16.25}$$

where $P$ are splitting functions that describe the probability of a given parton splitting into two others, and $n_f$ is the number of (active) quark flavors. The leading-order Altarelli-Parisi [16] splitting functions are

$$P_{qq} = \tfrac{4}{3}\left[\frac{1+x^2}{(1-x)}\right]_+ = \tfrac{4}{3}\left[\frac{1+x^2}{(1-x)_+}\right] + 2\delta(1-x)\ , \tag{16.26}$$

$$P_{qg} = \tfrac{1}{2}\left[x^2 + (1-x)^2\right]\ , \tag{16.27}$$

$$P_{gq} = \tfrac{4}{3}\left[\frac{1+(1-x)^2}{x}\right]\ , \tag{16.28}$$

$$P_{gg} = 6\left[\frac{1-x}{x} + x(1-x) + \frac{x}{(1-x)_+}\right] + \left[\frac{11}{2} - \frac{n_f}{3}\right]\delta(1-x), \tag{16.29}$$

where the notation $[F(x)]_+$ defines a distribution such that for any sufficiently regular test function, $f(x)$,

$$\int_0^1 dx f(x)[F(x)]_+ = \int_0^1 dx\ (f(x) - f(1))F(x)\ . \tag{16.30}$$

In general, the splitting functions can be expressed as a power series in $\alpha_s$. The series contains both terms proportional to $\ln\mu^2$ and to $\ln\ 1/x$. The leading-order DGLAP evolution sums up the $(\alpha_s \ln\mu^2)^n$ contributions, while at next-to-leading order (NLO) the sum over the $\alpha_s(\alpha_s \ln\mu^2)^{n-1}$ terms is included [18,19]. In fact, the NNLO contributions to the splitting functions and the DIS coefficient functions are now also all known [20,21,22].

In the kinematic region of very small $x$, it is essential to sum leading terms in $\ln\ 1/x$, independent of the value of $\ln\mu^2$. At leading order, LLx, this is done by the BFKL equation for the unintegrated distributions (see Refs. [23,24]) . The leading-order $(\alpha_s \ln(1/x))^n$ terms result in a power-like growth, $x^{-\omega}$ with $\omega = (12\alpha_s \ln 2)/\pi$, at asymptotic values of $\ln\ 1/x$. More recently, the next-to-leading $\ln\ 1/x$ (NLLx) contributions have become available [25,26]. They are so large (and negative) that the result appears to be perturbatively unstable. Methods, based on a combination of collinear and small $x$ resummations, have been developed which reorganize the perturbative series into a more stable hierarchy [27,28,29]. These studies show that the asymptotic properties of the small $x$ resummations are not significant at today's energies (which sample $x \gtrsim 10^{-4}$), and that in this domain NNLO DGLAP is a good approximation. Indeed, as yet, there is no firm evidence for any deviation from standard DGLAP evolution in the data for $Q^2 \gtrsim 2$ GeV$^2$. Nor is there any convincing indication that we have entered the 'non-linear' regime where the gluon density is so high that gluon-gluon recombination effects become significant.

The precision of the contemporary experimental data demands that NNLO (or at least NLO) DGLAP evolution be used in comparisons between QCD theory and experiment. At higher orders, it is necessary to specify, and to use consistently, both a renormalization and a factorization scheme. Whereas the renormalization scheme used is almost universally the modified minimal subtraction ($\overline{\text{MS}}$) scheme [30,31], there are two popular choices for factorization scheme, in which the form of the correction for each structure function is different. The two most-used factorization schemes are: DIS [32], in which there are no higher-order corrections to the $F_2$ structure function, and $\overline{\text{MS}}$ [33]. They differ in how the non-divergent pieces are assimilated in the parton distribution functions.

It is usually assumed that the quarks are massless. The effects of the $c$ and $b$-quark masses have been studied up to NNLO, for example, in Refs. 34–39. An approach using a variable flavor number is now generally adopted, in which evolution with $n_f = 3$ is matched to that with $n_f = 4$ at the charm threshold, with an analogous matching at the bottom threshold.

The discussion above relates to the $Q^2$ behavior of leading-twist (twist-2) contributions to the structure functions. Higher-twist terms, which involve their own non-perturbative input, exist. These die off as powers of $Q$; specifically twist-$n$ terms are damped by $1/Q^{n-2}$. The higher-twist terms appear to be numerically unimportant for $Q^2$ above a few GeV$^2$, except for $x$ close to 1.

**Table 16.1:** Lepton-nucleon and related hard-scattering processes and their primary sensitivity to the parton distributions that are probed.

| Process | Main Subprocess | PDFs Probed |
|---|---|---|
| $\ell^\pm N \to \ell^\pm X$ | $\gamma^* q \to q$ | $g(x \lesssim 0.01), q, \overline{q}$ |
| $\ell^+(\ell^-)N \to \overline{\nu}(\nu)X$ | $W^* q \to q'$ | |
| $\nu(\overline{\nu})N \to \ell^-(\ell^+)X$ | $W^* q \to q'$ | |
| $\nu\ N \to \mu^+\mu^- X$ | $W^* s \to c \to \mu^+$ | $s$ |
| $\ell N \to \ell Q X$ | $\gamma^* Q \to Q$ | $Q = c, b$ |
| | $\gamma^* g \to Q\overline{Q}$ | $g(x \lesssim 0.01)$ |
| $pp \to \gamma X$ | $qg \to \gamma q$ | $g$ |
| $pN \to \mu^+\mu^- X$ | $q\overline{q} \to \gamma^*$ | $\overline{q}$ |
| $pp, pn \to \mu^+\mu^- X$ | $u\overline{u}, d\overline{d} \to \gamma^*$ | $\overline{u} - \overline{d}$ |
| | $u\overline{d}, d\overline{u} \to \gamma^*$ | |
| $ep, en \to e\pi X$ | $\gamma^* q \to q$ | |
| $p\overline{p} \to W \to \ell^\pm X$ | $ud \to W$ | $u, d, u/d$ |
| $p\overline{p} \to$ jet $+X$ | $gg, qg, qq \to 2j$ | $q, g(0.01 \lesssim x \lesssim 0.5)$ |

## 16.3. Determination of parton distributions

The parton distribution functions (PDFs) can be determined from data for deep inelastic lepton-nucleon scattering and for related hard-scattering processes initiated by nucleons. Table 16.1 given below (based on Ref. [40]) highlights some processes and their primary sensitivity to PDFs.

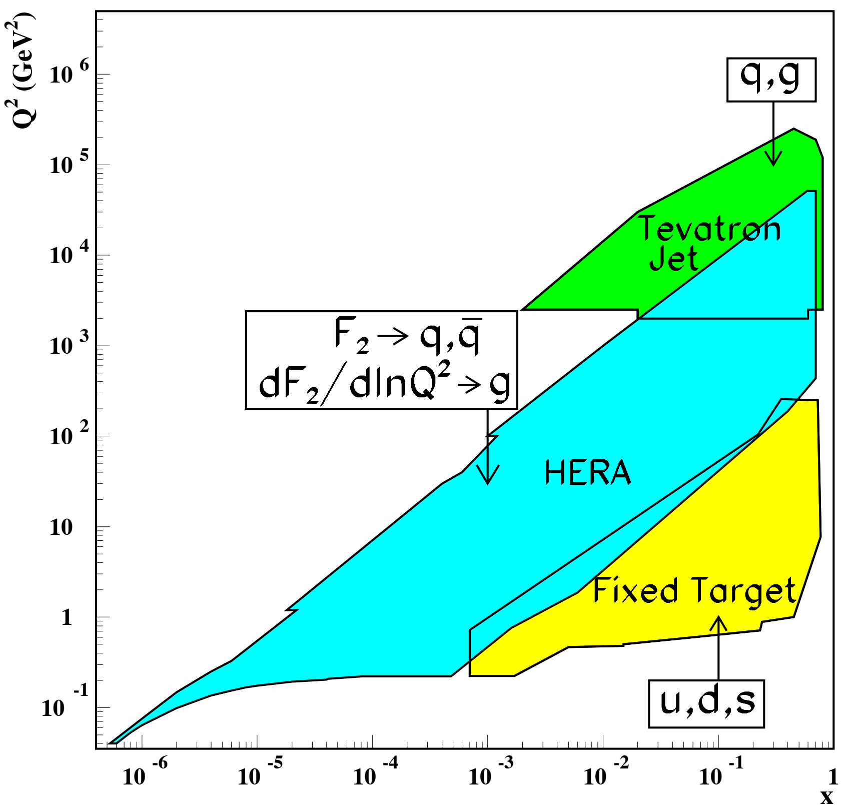


**Figure 16.3:** Kinematic domains in $x$ and $Q^2$ probed by fixed-target and collider experiments, shown together with the important constraints they make on the various parton distributions. See full-color version on color pages at end of book.

The kinematic ranges of fixed-target and collider experiments are complementary (as is shown in Fig. 16.3), which enables the determination of PDFs over a wide range in $x$ and $Q^2$. Recent determinations of the unpolarized PDF's from NLO global analyses are given in Ref. [13,41], and at NNLO in Ref. [13] (see also Ref. [42]) . Recent studies of the uncertainties in the PDFs and observables can be found in Refs. [43,44] and Refs. [45,46] (see also Ref. [47]) . The result of one analysis is shown in Fig. 16.4 at a scale $\mu^2 = 10$ GeV$^2$. The polarized PDFs are obtained through NLO global analyses of measurements of the $g_1$ structure function in inclusive polarized deep inelastic scattering (for recent examples see Refs. 48–50). The inclusive data do not provide enough observables to determine all polarized PDFs. These polarized PDFs may be fully accessed via flavor tagging in semi-inclusive deep inelastic scattering. Fig. 16.5 shows several global analyses at a scale of 2.5 GeV$^2$ along with the data from semi-inclusive DIS.

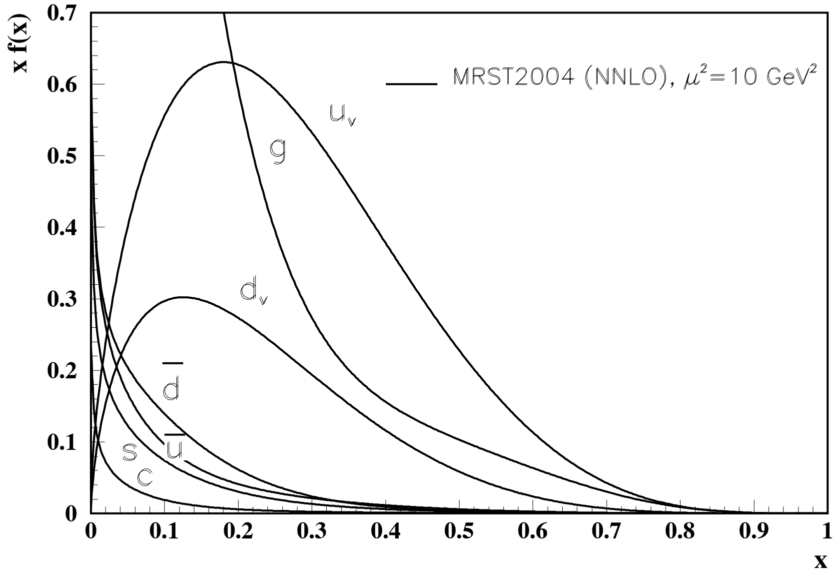


**Figure 16.4:** Distributions of $x$ times the unpolarized parton distributions $f(x)$ (where $f = u_v, d_v, \overline{u}, \overline{d}, s, c, g$) using the NNLO MRST2004 parameterization [13] at a scale $\mu^2 = 10$ GeV$^2$.

Comprehensive sets of PDFs available as program-callable functions can be obtained from several sources *e.g.*, Refs. [53,54]. As a result of a Les Houches Accord, a PDF package (LHAPDF) exists [55] which facilitates the inclusion of recent PDFs in Monte Carlo/Matrix Element programs in a very compact and efficient format.

## 16.4. DIS determinations of $\alpha_s$

Table 16.2 shows the values of $\alpha_S(M_Z^2)$ found in recent fits to DIS and related data in which the coupling is left as a free parameter.

There have been several other studies of $\alpha_s$ at NNLO, and beyond, using subsets of DIS data (see, for example, Refs. 59–61). Moreover, there exist global NLO analyses of polarized DIS data which give $\alpha_s(M_Z^2) = 0.120 \pm 0.009$ [62] and $0.114 \pm 0.009$ [50].

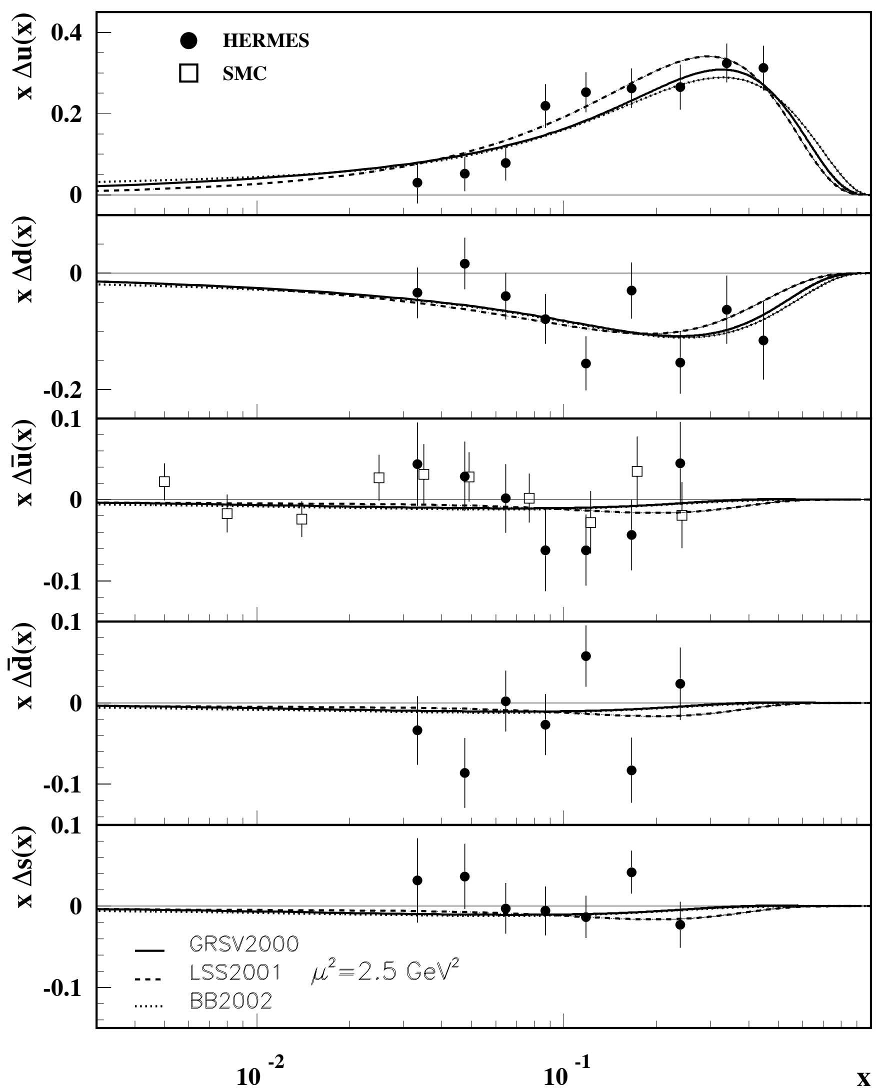


**Figure 16.5:** Distributions of $x$ times the polarized parton distributions $\Delta q(x)$ (where $q = u, d, \overline{u}, \overline{d}, s$) using the GRSV2000 [48], LSS2001 [49], and BB2002 [50] parameterizations at a scale $\mu^2 = 2.5\ \text{GeV}^2$. Points represent data from semi-inclusive positron (HERMES [51]) and muon (SMC [52]) deep inelastic scattering given at $Q^2 = 2.5\ \text{GeV}^2$. SMC results are extracted under the assumption that $\Delta\overline{u}(x) = \Delta\overline{d}(x)$.

## 16.5. The hadronic structure of the photon

Besides the *direct* interactions of the photon, it is possible for it to fluctuate into a hadronic state via the process $\gamma \to q\overline{q}$. While in this state, the partonic content of the photon may be *resolved*, for example, through the process $e^+e^- \to e^+e^-\gamma^*\gamma \to e^+e^-X$ where the virtual photon emitted by the DIS lepton probes the hadronic structure of the quasi-real photon emitted by the other lepton. The perturbative LO contributions,

**Table 16.2:** The values of $\alpha_S(M_Z^2)$ found in NLO and NNLO fits to DIS and related data. CTEQ [56] and MRST04 [13] are global fits. H1 [57] fit only a subset of the $F_2^{ep}$ data, while Alekhin [42] also includes $F_2^{ed}$ and ZEUS [58] in addition include their charged current and jet data. The experimental errors quoted correspond to different choices of the effective increase $\Delta\chi^2$ from the best fit value of $\chi^2$.

| | $\Delta\chi^2$ | $\alpha_S(M_Z^2)$ | $\pm$ expt | $\pm$ theory | $\pm$ model |
|---|---|---|---|---|---|
| NLO | | | | | |
| CTEQ | 37 | 0.1169 | $\pm$ 0.0045 | | |
| ZEUS | 50 | 0.1183 | $\pm$ 0.0028 | | $\pm$ 0.0008 |
| MRST04 | 20 | 0.1205 | $\pm$ 0.002 | $\pm$ 0.003 | |
| H1 | 1 | 0.115 | $\pm$ 0.0017 | $\pm$ 0.005 | $^{+0.0009}_{-0.0005}$ |
| Alekhin | 1 | 0.1171 | $\pm$ 0.0015 | $\pm$ 0.0033 | |
| NNLO | | | | | |
| MRST04 | 20 | 0.1167 | $\pm$ 0.002 | $\pm$ 0.003 | |
| Alekhin | 1 | 0.1143 | $\pm$ 0.0014 | $\pm$ 0.0009 | |

$\gamma \to q\bar{q}$ followed by $\gamma^* q \to q$, are subject to QCD corrections due to the coupling of quarks to gluons.

Often the equivalent-photon approximation is used to express the differential cross section for deep inelastic electron–photon scattering in terms of the structure functions of the transverse quasi-real photon times a flux factor $N_\gamma^T$ (for these incoming quasi-real photons of transverse polarization)

$$\frac{d^2\sigma}{dxdQ^2} = N_\gamma^T \frac{2\pi\alpha^2}{xQ^4} \left[ \left(1 + (1-y)^2\right) F_2^\gamma(x, Q^2) - y^2 F_L^\gamma(x, Q^2) \right],$$

where we have used $F_2^\gamma = 2xF_T^\gamma + F_L^\gamma$. Complete formulae are given, for example, in the comprehensive review of Ref. [63].

The hadronic photon structure function, $F_2^\gamma$, evolves with increasing $Q^2$ from the 'hadron-like' behavior, calculable via the vector-meson-dominance model, to the dominating 'point-like' behaviour, calculable in perturbative QCD. Due to the point-like coupling, the logarithmic evolution of $F_2^\gamma$ with $Q^2$ has a *positive* slope for all values of $x$, see Fig. 16.13. The 'loss' of quarks at large $x$ due to gluon radiation is over-compensated by the 'creation' of quarks via the point-like $\gamma \to q\bar{q}$ coupling. The logarithmic evolution was first predicted in the quark–parton model ($\gamma^*\gamma \to q\bar{q}$) [64,65] and then in QCD in the limit of large $Q^2$ [66]. The evolution is now known to NLO [67,68,69]. Recent NLO data analyses to determine the parton densities of the photon can be found in Refs. [70,71,72].

**References:**


1. J. Blümlein and N. Kochelev, Nucl. Phys. **B498**, 285 (1997).
2. S. Forte *et al.*, Nucl. Phys. **B602**, 585 (2001).
3. M. Anselmino *et al.*, Z. Phys. **C64**, 267 (1994).
4. M. Anselmino *et al.*, Phys. Rep. **261**, 1 (1995).
5. M. Klein and T. Riemann, Z. Phys. **C24**, 151 (1984).
6. C.G. Callan and D.J. Gross, Phys. Rev. Lett. **22**, 156 (1969).
7. D.A. Dicus, Phys. Rev. **D5**, 1367 (1972).
8. J.D. Bjorken and E.A. Paschos, Phys. Rev. **185**, 1975 (1969).
9. R.P. Feynman, Photon Hadron Interactions (Benjamin, New York, 1972).
10. S. Wandzura and F. Wilczek, Phys. Rev. **B72**, 195 (1977).
11. J. Blümlein and A. Tkabladze, Nucl. Phys. **B553**, 427 (1999).
12. J.D. Bjorken, Phys. Rev. **179**, 1547 (1969).
13. A.D. Martin *et al.*, Phys. Lett. **B604**, 61 (2004).
14. V.N. Gribov and L.N. Lipatov, Sov. J. Nucl. Phys. **15**, 438 (1972).
15. L.N. Lipatov, Sov. J. Nucl. Phys. **20**, 95 (1975).
16. G. Altarelli and G. Parisi, Nucl. Phys. **B126**, 298 (1977).
17. Yu.L. Dokshitzer, Sov. Phys. JETP **46**, 641 (1977).
18. G. Curci *et al.*, Nucl. Phys. **B175**, 27 (1980); W. Furmanski, and R. Petronzio, Phys. Lett. **B97**, 437 (1980).
19. R.K. Ellis *et al.*, QCD and Collider Physics (Cambridge UP, 1996).
20. E.B. Zijlstra and W.L. van Neerven, Phys. Lett. **B272**, 127 (1991); Phys. Lett. **B273**, 476 (1991); Phys. Lett. **B297**, 377 (1992); Nucl. Phys. **B383**, 525 (1992).
21. S. Moch and J.A.M. Vermaseren, Nucl. Phys. **B573**, 853 (2000).
22. S. Moch *et al.*, Nucl. Phys. **B688**, 101 (2004); Nucl. Phys. **B691**, 129 (2004); Phys. Lett. **B606**, 123 (2005); Nucl. Phys. **B724**, 3 (2005).
23. E.A. Kuraev *et al.*, Phys. Lett. **B60**, 50 (1975); Sov. Phys. JETP **44**, 443 (1976); Sov. Phys. JETP **45**, 199 (1977).
24. Ya.Ya. Balitsky and L.N. Lipatov, Sov. J. Nucl. Phys. **28**, 822 (1978).
25. V.S. Fadin, and L.N. Lipatov, Phys. Lett. **B429**, 127 (1998).
26. G. Camici and M. Ciafaloni, Phys. Lett. **B412**, 396 (1997), erratum-Phys. Lett. **B147**, 390 (1997); Phys. Lett. **B430**, 349 (1998).
27. M. Ciafaloni *et al.*, Phys. Rev. **D60**, 114036 (1999); JHEP **0007** 054 (2000).
28. M. Ciafaloni *et al.*, Phys. Lett. **B576**, 143 (2003); Phys. Rev. **D68**, 114003 (2003).
29. G. Altarelli *et al.*, Nucl. Phys. **B621**, 359 (2002); Nucl. Phys. **B674**, 459 (2003).
30. G. 't Hooft and M. Veltman, Nucl. Phys. **B44**, 189 (1972).
31. G. 't Hooft, Nucl. Phys. **B61**, 455 (1973).
32. G. Altarelli *et al.*, Nucl. Phys. **B143**, 521 (1978) and erratum: Nucl. Phys. **B146**, 544 (1978).
33. W.A. Bardeen *et al.*, Phys. Rev. **D18**, 3998 (1978).
34. M.A.G. Aivazis *et al.*, Phys. Rev. **D50**, 3102 (1994).
35. J.C. Collins, Phys. Rev. **D58**, 094002 (1998).
36. A. Chuvakin *et al.*, Phys. Rev. **D61**, 096004 (2000).

37. R.S. Thorne and R.G. Roberts, Phys. Rev. **D57**, 6871 (1998); Phys. Lett. **B421**, 303 (1998); Eur. Phys. J. **C19**, 339 (2001).
38. W.-K. Tung, *et al.*, J. Phys. **G28**, 983 (2002); S. Kretzer *et al.*, Phys. Rev. **D69**, 114005 (2004).
39. R.S. Thorne, Phys. Rev. **D73**, 054019 (2006).
40. A.D. Martin *et al.*, Eur. Phys. J. **C4**, 463 (1998).
41. CTEQ, J. Pumplin *et al.*, JHEP **0207**, 012 (2002).
42. S. Alekhin, JHEP **0302**, 015 (2003).
43. CTEQ, D. Stump *et al.*, Phys. Rev. **D65**, 014012 (2001).
44. CTEQ, J. Pumplin *et al.*, Phys. Rev. **D65**, 014013 (2001).
45. A.D. Martin *et al.*, Eur. Phys. J. **C28**, 455 (2003).
46. A.D. Martin *et al.*, Eur. Phys. J. **C35**, 325 (2004).
47. W.T. Giele *et al.*, `hep-ph/0104052`.
48. M. Glück *et al.*, Phys. Rev. **D63**, 094005 (2001).
49. E. Leader *et al.*, Eur. Phys. J. **C23**, 479 (2002).
50. J. Blümlein and H. Böttcher, Nucl. Phys. **B636**, 225 (2002).
51. HERMES, A. Airpetian *et al.*, Phys. Rev. Lett. **92**, 012005 (2004).
52. SMC, B. Adeva *et al.*, Phys. Lett. **B420**, 180 (1998).
53. H. Plothow-Besch, CERN PDFLIB, W5051 (2000).
54. `http://durpdg.dur.ac.uk/HEPDATA/PDF`.
55. `http://durpdg.dur.ac.uk/lhapdf/index.html`.
56. J. Huston *et al.*, JHEP **0506**, 080 (2005).
57. H1, C. Adloff *et al.*, Eur. Phys. J. **C21**, 33 (2001).
58. ZEUS, S. Chekanov *et al.*, Eur. Phys. J. **C42**, 1 (2005).
59. W.L. van Neerven and A. Vogt, Nucl. Phys. **B603**, 42 (2001).
60. J. Santiago and F.J. Yndurain, Nucl. Phys. **B611**, 447 (2001).
61. A.L. Kataev *et al.*, Phys. Part. Nucl. **34**, 20 (2003).
62. G. Altarelli *et al.*, Nucl. Phys. **B496**, 337 (1997).
63. R. Nisius, Phys. Reports **332**, 165 (2000).
64. T.F. Walsh and P.M. Zerwas, Phys. Lett. **B44**, 195 (1973).
65. R.L. Kingsley, Nucl. Phys. **B60**, 45 (1973).
66. E. Witten, Nucl. Phys. **B120**, 189 (1977).
67. W.A. Bardeen and A.J. Buras, Phys. Rev. **D20**, 166 (1979), erratum Phys. Rev. **D21**, 2041 (1980).
68. M. Fontannaz and E. Pilon, Phys. Rev. **D45**, 382 (1992), erratum Phys. Rev. **D46**, 484 (1992).
69. M. Glück *et al.*, Phys. Rev. **D45**, 3986 (1992).
70. F. Cornet *et al.*, Phys. Rev. **D70**, 093004 (2004).
71. P. Aurenche, *et al.*, Eur. Phys. J. **C44**, 395 (2005).
72. W. Slominski *et al.*, Eur. Phys. J. **C45**, 633 (2006).